Available online at www.sciencedirect.com
ScienceDirect
Journal of Sound and Vibration 323 (2009) 790–801
JOURNAL OF SOUND AND VIBRATION
www.elsevier.com/locate/jsvi

The coupled dynamics of two cantilevered flexible plates in axial flow

Liaosha Tang[a,*], Michael P. Païdoussis[b]

[a]University of Toronto, Institute for Aerospace Studies, 4925 Dufferin St., Toronto, Ontario, Canada M3H 5T6
[b]Department of Mechanical Engineering, McGill University, 817 Sherbrooke St. W., Montréal, Québec, Canada H3A 2K6

Received 5 May 2008; received in revised form 20 November 2008; accepted 14 January 2009
Handling Editor: S. Bolton
Available online 26 February 2009

Abstract

This paper studies the coupled dynamics of two cantilevered flexible plates aligned parallel to each other in axial flow. The nonlinear governing equation of the two-dimensional plate is developed using the inextensibility condition; and an unsteady lumped vortex model, taking into account the interactions between the two plates, is used to calculate the pressure difference across each plate. The analysis of the system dynamics is carried out in the time-domain; both the instability and the post-critical behaviour are investigated. It is found that the system loses stability through flutter when the flow velocity is sufficiently high, and the flutter threshold is a function of the separation between the two plates. It is also found that the two plates may oscillate both in the out-of-phase and in-phase modes; the former always has a lower critical point than the latter. Moreover, flutter of the two-plate system in the in-phase mode is proved to be associated with an unstable branch of the solution, which can be obtained through numerical simulations with the aid of so-called virtual spring connections.

1. Introduction

The dynamics of a single two-dimensional cantilevered thin flexible plate in axial flow and variants of this fluid–structure system has been reviewed extensively by Tang [1], Tang and Païdoussis [2,3], and Tang et al. [4]. The system may lose stability at sufficiently high flow velocity. Once the critical point is exceeded, flutter takes place, and the amplitude of the symmetrical limit cycle oscillations grows as the flow velocity increases further. This paper studies the coupled dynamics of two cantilevered flexible plates aligned parallel to each other in axial flow, which can be regarded as a new variant of the one-plate system investigated before.

Rectangular parallel-plate assemblies are used as core elements of nuclear reactors, and the hydroelastic instability of this system has recently been studied by Guo and Païdoussis [5]. In their work, the plates are assumed to be clamped along the side-wall, while the inlet and outlet edges are free; the fluid flows inside the channels formed by the parallel-plate assembly and the side-walls. In the analysis of the parallel-plate

*Corresponding author. Tel.: +1 416 6677701; fax: +1 416 6677799.
E-mail address: ltang2008@gmail.com (L. Tang).

0022-460X/$ - see front matter © 2009 Elsevier Ltd. All rights reserved.
doi:10.1016/j.jsv.2009.01.028

assemblies, it is normally *a priori* assumed, as supported by experimental observations, that all plates have the same deflection and modal shape at any time, but two adjacent plates deflect in opposite directions; that is, the divergence or flutter of the plates are supposed to be in the out-of-phase mode. Zhang et al. [6] examined experimentally the coupled states of two clamped filaments in a flowing soap film for studying one-dimensional flags (i.e., flexible plates) in two-dimensional wind. Flutter in both the in-phase and out-of-phase modes are observed, and the oscillation modes are found to be dependent on the separation between the two filaments: at a fixed, sufficiently high flow velocity, the two filaments oscillate in phase when the separation is small, but out of phase as the separation is increased. Some of the experimental observations made by Zhang et al. [6] have preliminarily been confirmed by the theoretical work of Farnell et al. [7], who use a Navier–Stokes solver for the aero/hydro-dynamics and model each flexible plate as a so-called *N-tuple pendulum* for two two-dimensional cantilevered flexible plates in axial channel flow (the fluid domain is confined by the upper/lower channel walls).

In this paper, the dynamics of cantilevered flexible plates in axial *open* flow, instead of *channel* flow, is studied, unlike the work by Zhang et al. [6] and Farnell et al. [7]. The two-dimensional plate is modelled as a beam with an inextensible centreline, and an unsteady lumped vortex model, taking into account the interactions between the two plates, is used to calculate the pressure difference across each plate. The analysis is carried out in the time-domain, and both the instability and post-critical behaviour of the two-plate system are investigated. It is found that the two plates can oscillate in both the in-phase and out-of-phase modes. However, only the oscillations in the out-of-phase mode are stable; they can naturally be obtained through numerical simulations based on the original model. In order to obtain in-phase oscillations, a new technique called the virtual-spring-connection method is adopted.

It should be mentioned that the current research has not only originated from theoretical curiosity but is also related to the design of a new type energy-harvesting device [1], i.e., the ''flutter-mill'', where two or more cantilevered flexible plates aligned parallel to each other in axial flow may be considered.

2. The aero/hydro-elastic model

2.1. One-plate system

A schematic diagram of a single cantilevered flexible plate in open axial flow is shown in Fig. 1. The geometrical characteristics of the rectangular homogeneous plate are the length of the flexible section L, width B and thickness h; $B \to \infty$ and $h \ll L$ for a two-dimensional thin plate. Normally, there is a rigid segment of length L_0 as part of the clamping arrangement at the upstream end. The other physical parameters of the system are: the plate material density ρ_P and bending stiffness $D = Eh^3/\sqrt{12(1-\nu^2)}$, where E and ν are, respectively, Young's modulus and the Poisson ratio of the plate material, the fluid density ρ_F, and the undisturbed flow velocity U. As shown in Fig. 1, W and V are, respectively, the transverse and longitudinal displacements of the plate; F_L and F_D are, respectively, the aero/hydro-dynamic loads acting on the plate in the transverse and longitudinal directions, respectively; and S is the distance of a material point on the plate from the origin, measured along the plate centreline in a coordinate system embedded in the plate. Moreover, material damping of the Kelvin–Voigt type is considered with the loss coefficient denoted by a.

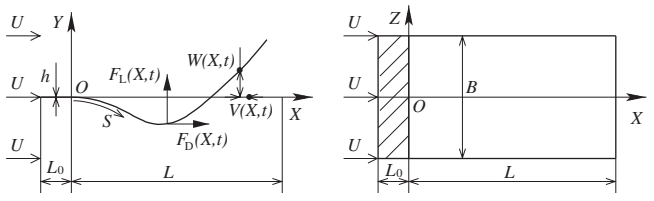

Fig. 1. A single cantilevered flexible plate in open axial flow.

The equations of motion of the plate can be written in nondimensional form as [2]

$$\ddot{w}+\left(1+\alpha\frac{\partial}{\partial\tau}\right)[w''''(1+w'^2)+4w'w''w'''+w''^3]+w'\int_0^s(\dot{w}'^2+w'\ddot{w}')\,\mathrm{d}s-w''\int_s^1\left[\int_0^s(\dot{w}'^2+w'\ddot{w}')\,\mathrm{d}s\right]\mathrm{d}s=f_{\mathrm{eff}},\tag{1}$$

$$v=-\frac{1}{2}\int_0^s w'^2\,\mathrm{d}s,\tag{2}$$

$$f_{\mathrm{eff}}=\mu U_R^2\left(f_L-w'f_D+w''\int_s^1 f_D\,\mathrm{d}s\right),\tag{3}$$

where the overdot and the prime represent $\partial(\,)/\partial\tau$ and $\partial(\,)/\partial s$, respectively. The nondimensional variables are defined by

$$\begin{aligned}&x=\frac{X}{L},\quad y=\frac{Y}{L},\quad w=\frac{W}{L},\quad v=\frac{V}{L},\quad s=\frac{S}{L},\quad l_0=\frac{L_0}{L},\\&\tau=\frac{t}{\sqrt{\rho_P hL^4/D}},\quad \alpha=\frac{a}{\sqrt{\rho_P hL^4/D}},\quad f^\star=f\sqrt{\rho_P hL^4/D},\\&f_L=\frac{F_L}{\rho_F U^2},\quad f_D=\frac{F_D}{\rho_F U^2},\end{aligned}\tag{4}$$

where $f^\star$ and f are, respectively, nondimensional and dimensional oscillation frequencies. Moreover, the mass ratio μ and the reduced flow velocity U_R are, respectively, defined by

$$\mu=\frac{\rho_F L}{\rho_P h},\quad U_R=UL\sqrt{\frac{\rho_P h}{D}}.\tag{5}$$

In Eq. (3), the aero/hydro-dynamic loads are calculated using the unsteady lumped vortex model [2]. In particular, the flexible plate is evenly divided into N panels, each of length $\Delta s=1/N$. Individual panels are put on the deformed contour of the plate centreline. The bound vortices, γ_1 through γ_N, together with the instantaneously formed wake vortex γ_{N+1} at a given instant, say time step $k+1$, are obtained from the following equations:

$$\begin{bmatrix}\alpha_{11}&\alpha_{12}&\cdots&\alpha_{1N}&\alpha_{1,N+1}\\\alpha_{21}&\alpha_{22}&\cdots&\alpha_{2N}&\alpha_{2,N+1}\\\vdots&\vdots&\ddots&\vdots&\vdots\\\alpha_{N1}&\alpha_{N2}&\cdots&\alpha_{NN}&\alpha_{N,N+1}\\1&1&\cdots&1&1\end{bmatrix}\begin{Bmatrix}\gamma_1\\\gamma_2\\\vdots\\\gamma_N\\\gamma_{N+1}\end{Bmatrix}=\begin{Bmatrix}\mathrm{rhs}_1\\\mathrm{rhs}_2\\\vdots\\\mathrm{rhs}_N\\\gamma^\star\end{Bmatrix},\tag{6}$$

where the influence coefficients α_{ij} and the right-hand side $\{\mathrm{rhs}_i,\gamma^\star\}^{\mathrm{T}}$ are given by

$$\alpha_{ij}=\frac{(y_{Ci}-y_{Vj})\sin\alpha_i+(-x_{Ci}+x_{Vj})\cos\alpha_i}{2\pi[(y_{Ci}-y_{Vj})^2+(x_{Ci}-x_{Vj})^2]},\tag{7}$$

$$\mathrm{rhs}_i=\left(\frac{\dot{v}_i}{U_R}-1-v_{Wi}\right)\sin\alpha_i+\left(\frac{\dot{w}_i}{U_R}-w_{Wi}\right)\cos\alpha_i,\tag{8}$$

$$\gamma^{\star k+1}=\sum_{i=1}^{N}\gamma_i^k.\tag{9}$$

In Eq. (6), $\gamma_{i,i=1,2,\ldots,N}$ and γ_{N+1} are, respectively, the strengths of the bound vortices $\Gamma_{i,i=1,2,\ldots,N}$ and the latest wake vortex Γ_{W1} normalized by UL. In Eqs. (7) and (8), $(x,y)_{Ci}$ and $(x,y)_{Vi}$ are, respectively, the coordinates of the bound vortex and the collocation point on the ith panel $(X,Y)_{Ci}$ and $(X,Y)_{Vi}$ normalized by L; $(v,w)_{Wi}$

is the wake-induced velocity at the ith collocation point $(V, W)_{W_i}$ normalized by the undisturbed flow velocity U. In Eq. (9), the superscript $k+1$ represents the current time step; it has been dropped for clarity in Eqs. (6)–(8).

The truncated wake street is assumed to have a normalized longitudinal length l_W ($l_W = L_W/L$), and the total number of wake vortices N_W can be determined by $N_W = l_W/(U_R\Delta\tau)$. Thus, the wake-induced velocity at the ith collocation point is calculated by

$$(v, w)_{W_i} = \sum_{j=1}^{N_W} \frac{\gamma_{Wj}}{2\pi} \frac{(y_{Ci} - y_{Wj}, -x_{Ci} + x_{Wj})}{(y_{Ci} - y_{Wj})^2 + (x_{Ci} - x_{Wj})^2}, \tag{10}$$

where γ_{Wi} and $(x, y)_{Wj}$ are, respectively, the strength and coordinates of the jth wake vortex Γ_{Wj} normalized by UL and $(X, Y)_{Wj}$ by L.

When discrete vortices γ_1 through γ_{N+1} are available at the current time step, Δp_i, the pressure difference at the ith panel (ΔP_i normalized by $\rho_F U^2$), can be calculated by the following expression [8]:

$$\Delta p_i = \left[\left(-\frac{\dot{v}_i}{U_R} + 1 + v_{Wi}\right)\cos\alpha_i + \left(\frac{\dot{w}_i}{U_R} - w_{Wi}\right)\sin\alpha_i\right]\frac{\gamma_i}{\Delta s} + \frac{1}{U_R}\frac{\partial}{\partial\tau}\left(\sum_{j=1}^{i}\gamma_j\right). \tag{11}$$

Consequently, the distributions of the *lift* f_{Li} and the *drag* f_{Di} over the ith panel are obtained by

$$f_{L_i} = \Delta p_i \cos\alpha_i, \quad f_{Di} = \Delta p_i \sin\alpha_i + C_D, \tag{12}$$

where α_i is the incidence angle of the ith panel. An additional drag coefficient C_D, assumed to be uniformly distributed over the whole length of the plate, may be considered in f_D to account for the *viscous* effects of the fluid flow.

2.2. Two-plate system: the original model

When there are two identical cantilevered flexible plates aligned parallel two each other, as shown in Fig. 2 in open axial flow, it is assumed that the two plates originally lie along the X^1 and X^2 axes, respectively; the distance between X^1 and X^2 is D_P, or d_P when normalized using L. The fixed $X-Y$ coordinate system is based on the first plate, coinciding with the X^1-Y^1 system. Therefore, the two plates have the same equations of motion, namely Eqs. (1) and (2), except that the transverse displacements of the second plate $w^2(s)$ include a fixed constant part, d_P.

The system involving multiple cantilevered flexible plates in axial flow may be categorized as a blade–blade interaction problem [9], which is concerned with the interactions of multiple airfoils/wings in either the aligned-in-parallel configuration or the tandem configuration. Jones and Platzer [10] solved the two-airfoil-in-tandem problem without considering the impingement of the vortices shed from the upstream airfoil upon the downstream one. Improved schemes were developed by Jones and Platzer [11] and Yao and Liu [9] to prevent any moving vortex from penetrating into the body of the (downstream) finite-thickness airfoil. However, in the current problem of two thin plates (of sensibly "zero" thickness) aligned parallel to each other

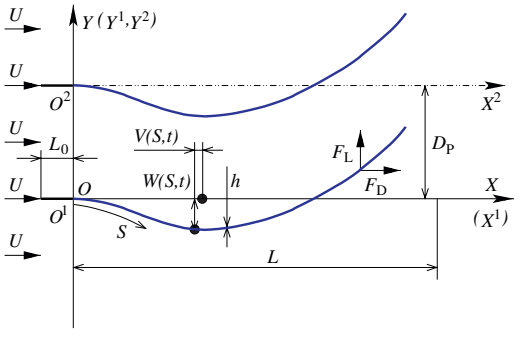

Fig. 2. Two identical cantilevered flexible plates aligned parallel to each other in axial flow.

in axial flow, it is not necessary to consider such vortex impingement because the vortices shed from the trailing edge of either plate never approach the other one.

As for the aero/hydro-dynamics part of the two-plate system, following the scheme utilized by Yao and Liu [9], the bound vortices and the latest wake vortices of both plates are simultaneously solved, while satisfying the Kutta–Joukowski condition and Kelvin's theorem for either plate, from

$$\begin{bmatrix} \mathbf{A}^{1,1} & \mathbf{A}^{1,2} \\ \mathbf{A}^{2,1} & \mathbf{A}^{2,2} \end{bmatrix} \begin{Bmatrix} \mathscr{V}^1 \\ \mathscr{V}^2 \end{Bmatrix} = \begin{Bmatrix} \mathscr{R}^1 \\ \mathscr{R}^2 \end{Bmatrix}, \tag{13}$$

where $\mathbf{A}^{m,n}$ $(m = 1, 2,\ n = 1, 2)$ is the matrix of influence coefficients of plate n on plate m, which is defined by (refer to Eq. (6))

$$\mathbf{A}^{m,n} = \begin{bmatrix} \alpha_{m_1,n_1} & \alpha_{m_1,n_2} & \cdots & \alpha_{m_1,n_N} & \alpha_{m_1,n_{N+1}} \\ \alpha_{m_2,n_1} & \alpha_{m_2,n_2} & \cdots & \alpha_{m_2,n_N} & \alpha_{m_2,n_{N+1}} \\ \vdots & \vdots & \ddots & \vdots & \vdots \\ \alpha_{m_N,n_1} & \alpha_{m_N,n_2} & \cdots & \alpha_{m_N,n_N} & \alpha_{m_N,n_{N+1}} \\ \delta_{m,n} & \delta_{m,n} & \cdots & \delta_{m,n} & \delta_{m,n} \end{bmatrix}. \tag{14}$$

In Eq. (14), $\delta_{m,n}$ is the Dirac delta function, and α_{m_i,n_j} is calculated by

$$\alpha_{m_i,n_j} = \frac{(y_{C_i}^m - y_{V_j}^n)\sin\alpha_i^m + (-x_{C_i}^m + x_{V_j}^n)\cos\alpha_i^m}{2\pi[(y_{C_i}^m - y_{V_j}^n)^2 + (x_{C_i}^m - x_{V_j}^n)^2]}. \tag{15}$$

In Eq. (13), $\mathscr{V}^m$ $(m = 1, 2)$ is the vector consisting of the bound vortices γ_i^m $(i = 1, 2, \ldots, N)$ and the latest wake vortex γ_{N+1}^m of plate m, and $\mathscr{R}^m$ is the right-hand-side vector of plate m; they are, respectively, defined by

$$\mathscr{V}^m = \{\gamma_1^m, \gamma_2^m, \ldots, \gamma_N^m, \gamma_{N+1}^m\}^{\mathrm{T}}, \tag{16}$$

$$\mathscr{R}^m = \{\mathrm{rhs}_1^m, \mathrm{rhs}_2^m, \ldots, \mathrm{rhs}_N^m, \gamma^{\star m}\}^{\mathrm{T}}, \tag{17}$$

where

$$\mathrm{rhs}_i^m = \left(\frac{\dot{v}_i^m}{U_R} - 1 - v_{W_i}^m\right)\sin\alpha_i^m + \left(\frac{\dot{w}_i^m}{U_R} - w_{W_i}^m\right)\cos\alpha_i^m, \tag{18}$$

$$\gamma^{\star m;k+1} = \sum_{i=1}^{N} \gamma_i^{m;k}. \tag{19}$$

In Eq. (18), $(v, w)_{W_i}^m$ is the wake-induced flow velocity at the ith collocation point of plate m, which should be calculated by

$$(v, w)_{W_i}^m = \sum_{n=1}^{2}\sum_{j=1}^{N_W} \frac{\gamma_{W_j}^n}{2\pi} \frac{(y_{C_i}^m - y_{W_j}^n, -x_{C_i}^m + x_{W_j}^n)}{(y_{C_i}^m - y_{W_j}^n)^2 + (x_{C_i}^m - x_{W_j}^n)^2}, \tag{20}$$

that is, the wakes of both plates should be considered in the calculation of the wake-induced flow velocity $(v, w)_{W_i}^m$.

When the distribution of the discrete vortices on each plate is available, the pressure difference across plate m can be calculated by (refer to Eq. (11))

$$\Delta p_i^m = \left[\left(-\frac{\dot{v}_i^m}{U_R} + 1 + v_{W_i}^m + v_{\Gamma_i}^m\right)\cos\alpha_i^m \left(\frac{\dot{w}_i^m}{U_R} - w_{W_i}^m - w_{\Gamma_i}^m\right)\sin\alpha_i^m\right]\frac{\gamma_i^m}{\Delta s} + \frac{1}{U_R}\frac{\partial}{\partial\tau}\left(\sum_{j=1}^{i}\gamma_j^m\right), \tag{21}$$

and then Eq. (12) is used to calculate the fluid loads $f_{L_i}^m$ and $f_{D_i}^m$ acting on plate m. Note that, in Eq. (21), the wake-induced flow velocity $(v, w)_{W_i}^m$ should be calculated according to Eq. (20), and the flow velocity induced

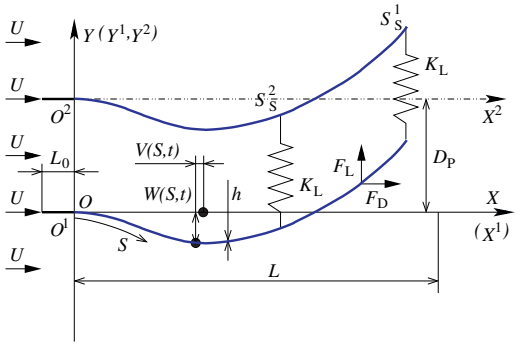

Fig. 3. Two identical cantilevered flexible plates aligned parallel to each other in axial flow with virtual spring connections.

by the bound vortices on the other plate n, i.e., $(v,w)_{\Gamma_i^m}$, calculated by

$$(v,w)_{\Gamma_i^m}=\sum_{j=1}^{N}\frac{\gamma_{V_j^n}}{2\pi}\frac{(y_{C_i^m}-y_{V_j^n},-x_{C_i^m}+x_{V_j^n})}{(y_{C_i^m}-y_{V_j^n})^2+(x_{C_i^m}-x_{V_j^n})^2}, \tag{22}$$

should also be considered.

2.3. Two-plate system: the in-phase model

Besides the original model developed for the two-plate system, an in-phase model is also considered. That is, as shown in Fig. 3, two virtual spring connections are introduced, and the *lift* force acting on plate m, now denoted as $\overline{f_L}$, should be calculated by

$$\overline{f_{Li}}^m=f_{Li}^m\pm k_L(w^2-w^1-d_P)\delta(s-s_S^1)\pm k_L(w^2-w^1-d_P)\delta(s-s_S^2), \tag{23}$$

where k_L is the spring stiffness normalized by L^4/D [3]; $s_S^{1,2}$ are the spring locations normalized by L. Note that, the "+" sign is used when $m=1$; while, the "−" sign when $m=2$.

The consideration of the virtual spring connections is supposed to force the two plates to always oscillate in phase. When they indeed oscillate in phase, the distance between the two plates everywhere along the whole length of the plates is exactly d_P, and $w^2-w^1-d_P\equiv 0$; that is, no spring force acts on the plates. The value of the spring stiffness k_L should be sufficiently large in order to avoid the springs influencing the dynamics of the system. In the current investigation, $k_L=1.0\times 10^6$ is used; refer to the dynamics of the one-plate system with an additional spring support studied in Ref. [3], where much smaller values of k_L are considered. Moreover, the number and location of the spring connections are determined by the dynamics of the corresponding one-plate system: when the mass ratio μ of the one-plate system is small, say $\mu<0.6$, the plate oscillates in the second beam mode and a quasi-node can be observed at about three-quarters of the plate length; therefore, the two virtual connections can be placed at $s_S^1=1$ and $s_S^2=0.75$.

3. The dynamics of the two-plate system

In the present paper, one is specifically interested in the in-phase and out-of-phase modes of the two-plate system, and the parameters $\mu=0.2$, $l_0=0.01$,[1] $\alpha=0.004$ and $C_D=0$ are uniformly used in the analysis, as the dynamics of the one-plate system with the same parameters has been investigated extensively in Ref. [2], and the influence of the parameters l_0, α or C_D on the dynamics has also been studied therein.

In particular, the flutter boundaries of the two-plate system, respectively, obtained using the original model (without constraining springs) and the in-phase model (with springs), are presented in Fig. 4(a). It can be seen

[1]The parameter $l_0=0.01$ represents a basic case where the upstream clamping constraint effectively has no length. In practice, using $l_0=0.01$ instead of $l_0=0$ in the present paper and Ref. [2] is a small trick for the purpose of avoiding the leading edge singularity in the aerodynamic calculations involved.

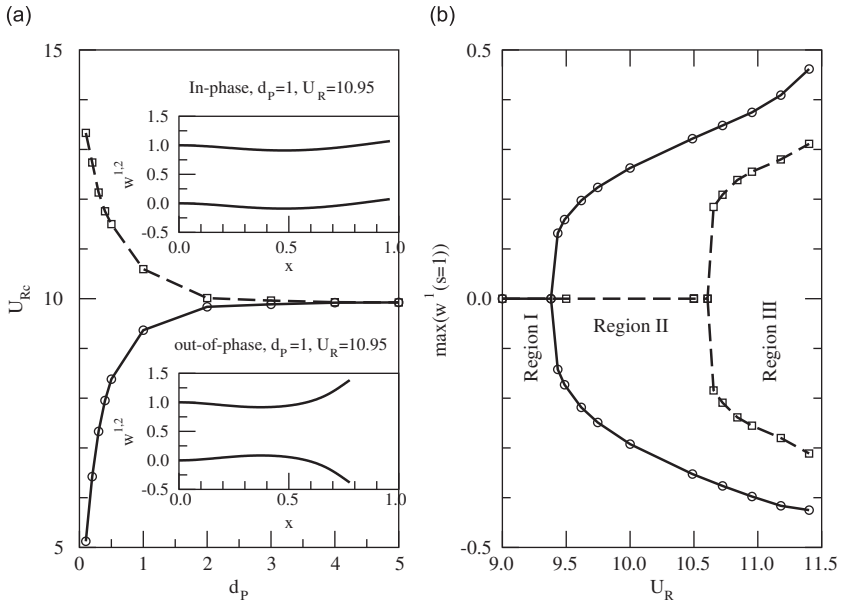

Fig. 4. (a) The instability boundary of the two-plate system in terms of d_P, and (b) the bifurcation diagram of the two-plate system with $d_P = 1$. Solid line with circles, the original model; dashed line with squares, the in-phase model.

that the system oscillating in phase is always more stable than the system oscillating out of phase, as the original model predicts a flutter boundary below the one obtained using the in-phase model. When d_P is small, the stability of the system depends on the separation distance of the two plates; the smaller the value of d_P, the more significant is its influence. On the other hand, when $d_P = 5$, no difference can found between the original model and the in-phase model, as well as between the models of the two-plate system and the one-plate system, in that all of them predict the same critical reduced flow velocity at $U_{Rc} = 9.92$. One can also see in Fig. 4(a) that, as compared to the one-plate system, with decreasing values of d_P, the two-plate system becomes increasingly less stable when it oscillates in the out-of-phase mode; while, on the contrary, increasingly more stable in the in-phase mode. It should be mentioned that the two plates oscillating out-of-phase can be viewed as a case of a single plate in the presence of a ground plane, with the ground surface coinciding with the mid-plane of the two plates, i.e., the $y = d_P/2$ plane; the other plate is just the mirror-image of the first one with respect to the ground surface.[2] With the ground effect, a larger aero/hydro-dynamic load (*lift*) can beexpected, and the plate becomes less stable.

It should be emphasized that the spring connections considered in the in-phase model are virtual ones; no spring forces act on the plates when the plate oscillates in-phase because the separation between the two plates is always d_P (the original length of the springs). Through extensive tests, it was found that in-phase solutions cannot be obtained using the original model. Moreover, if while working with the in-phase model the virtual spring connections are broken in the middle of the numerical simulation after a stable in-phase solution has already been achieved, one finds that the dynamics of the two-plate system (in-phase oscillations) is altered and finally converges to the dynamics obtained by using the original model (out-of-phase oscillations).

[2]Let us look at a one-plate system in association with a ground plane located at $y = d_p/2$. This new problem may be solved using a distribution of vortex type singularities for the plate as well as the downstream wake. When taking into account the ground plane, each individual vortex has its own mirror image with the ground plane as the mirror (i.e., the plane of symmetry). The distribution of these mirrored vortices actually constitutes a mirrored plate and its own wake. Moreover, we need to solve the original and mirrored plates and wakes simultaneously for the one-plate system with the presence of a ground plane, just as we did in the solution of the two-plate system. The only difference is this: in the former problem we assume *a priori* that the original and mirrored plates oscillate in the out-of-phase mode, while in the latter problem we know *a posteriori* that the two plates indeed oscillate out of phase. Therefore, the two problems are actually identical and, when stable limit cycle oscillations have been well established (i.e., the solution of either the former or the latter problem) the mutual aerodynamic influence between the original and mirrored plates in the former problem and that between the two plates in the latter problem are exactly the same.

As shown in Fig. 4(b), two bifurcation diagrams are obtained using (i) the original model and (ii) the in-phase model for the case $d_P = 1$. Because the spring connections considered are virtual ones, the in-phase model is indeed identical to the original model when the two plates oscillate in-phase. Therefore, the two bifurcation diagrams shown in Fig. 4(b) can be viewed as a combined one for the two-plate system. That is, the in-phase state of the system is the unstable branch (denoted by the dashed-line), which cannot be predicted by the original model, but which can nevertheless be captured with the aid of the virtual spring connections (i.e., using the in-phase model). It should be mentioned that between the two critical points, respectively, predicted by the original model and the in-phase model, the stretched-straight state of the two plates is also an unstable branch. Therefore, the dynamics of the two-plate system can be divided into three regions as U_R is increased: (i) region I, involving only the stable flat state, (ii) region II, where a stable limit cycle and an unstable flat state coexist, and (iii) region III, where stable and unstable limit cycle oscillations coexist.

Both the original and in-phase models have been studied with various initial conditions, either in-phase or out-of-phase. With out-of-phase initial conditions, the virtual springs in the in-phase model become effective and, after the transients have died out, in-phase oscillations result, as expected. On the other hand, without the virtual springs, the original model always predicts out-of-phase oscillations, no matter what initial conditions are used, as shown in Figs. 5(a) and (b) for $d_P = 1$ and $U_R = 10$. It is of interest to observe in Fig. 5(b) that the two plates always oscillate out-of-phase if they are started with out-of-phase initial conditions. In contrast, as shown in Fig. 5(a), when in-phase initial conditions are used, the phase relationship is gradually reorganized and eventually out-of-phase oscillation results; a longer transient, as compared to the dynamics shown in Fig. 5(b), can be observed in Fig. 5(a) due to this phase reorganization process.

The evolution of the phase relationship between the two plates can be seen more clearly in Fig. 6, in the case of $d_P = 3$ and $U_R = 9.9$, obtained by means of the original model with in-phase initial conditions. Note that, for $d_P = 3$, the critical points of the original and in-phase models are, respectively, $U_{Rc} = 9.87$ and 9.95. These two critical points are very close to each other because the coupling between the two plates is attenuated as a result of the large d_P involved. Therefore, for the results of Fig. 6, the reduced flow velocity U_R is close to the

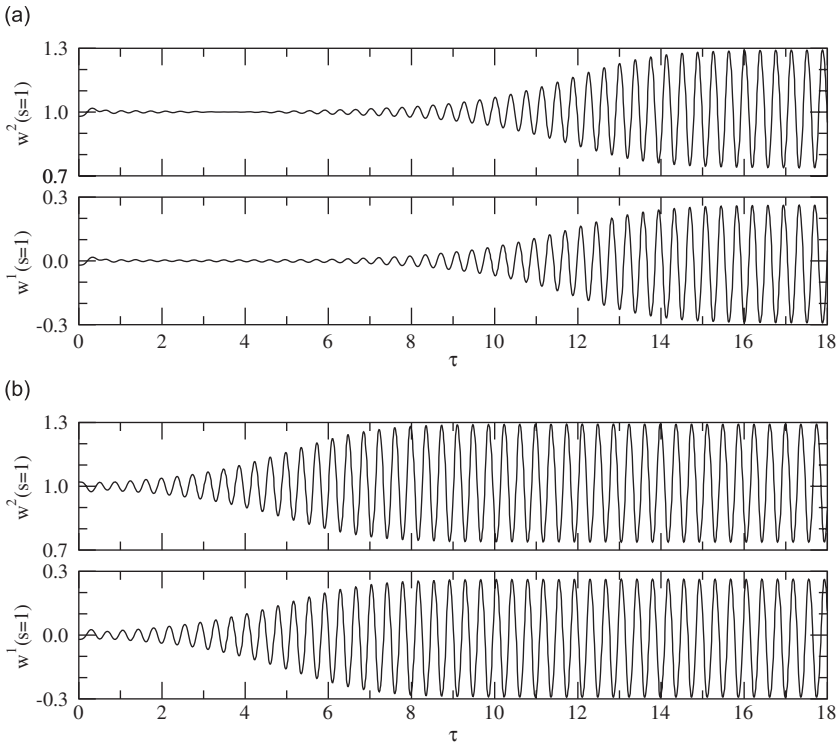

Fig. 5. The time histories of the two-plate system with $d_P = 1$ obtained using the original model with (a) in-phase and (b) out-of-phase initial conditions.

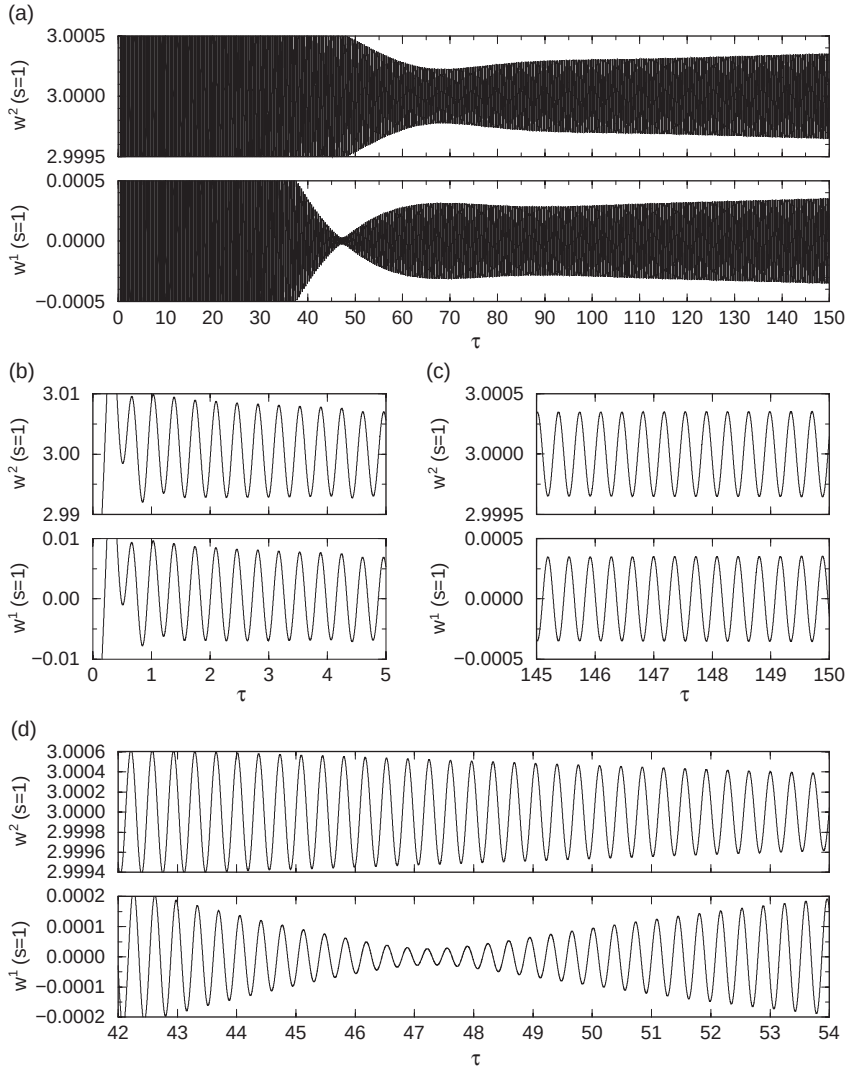

Fig. 6. (a) The time history of the two-plate system with $d_P = 3$ obtained using the original model with in-phase initial conditions at $U_R = 9.9$; and (b–d) various segments of the time history shown in (a).

critical point; as one can see in Fig. 6(a), there is a long transient, as expected. At the beginning, since in-phase initial conditions have been used, the two plates oscillate in-phase with the same amplitude, as shown in Fig. 6(b). Moreover, because $U_R = 9.9$ is below the in-phase critical point, the oscillation amplitudes of the plates decrease. As time elapses, a phase difference between the two plates emerges and grows, as shown in Fig. 6(d). During the process of phase reorganization, the oscillation amplitudes of the two plates are different. Additionally, as the oscillation amplitude of one plate decreases with time that of the other one increases. A close examination of Fig. 6(d) reveals that the transition from in-phase motions to out-of-phase motions is not achieved at one stroke from 0 (in-phase) to π (out-of-phase) in terms of phase difference. For example, a significant phase difference can be observed for $42<\tau<43$ and $53<\tau<54$, while the two plates oscillate almost in-phase for $47<\tau<48$. Nevertheless, when a sufficiently long time has elapsed, the two plates at last oscillate out of phase (a phase difference of π) with the same amplitude, as shown in Fig. 6(c). Finally, because the current U_R is larger than the out-of-phase critical point, the oscillation amplitudes of both plates grow (note that the time histories of Fig. 6(a) show that the system is still in a transient state).

The post-critical dynamics of the two-plate system are studied in Fig. 7 for $d_P = 1$ and $U_R = 10.95$, where both the original and in-phase models predict limit cycle oscillations (see Fig. 4(a) and region III in Fig. 4(b)).

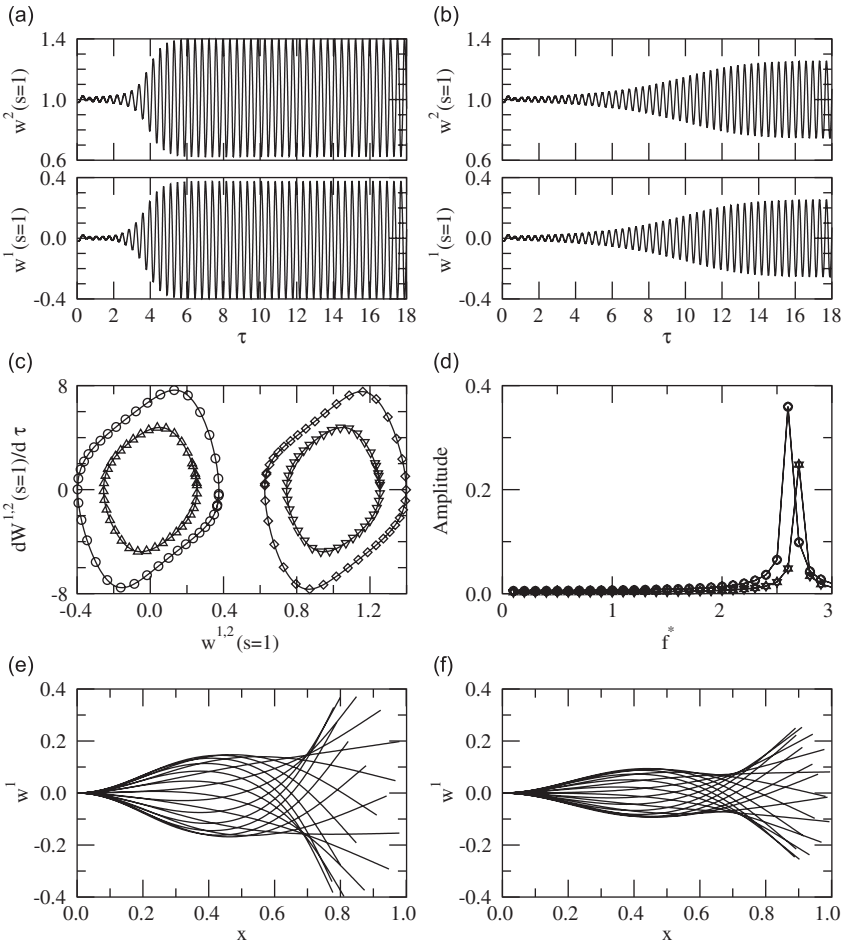

Fig. 7. The post-critical behaviour of the two-plate system obtained by the original and in-phase models with the parameters $d_P = 1$ and $U_R = 10.95$: the time history obtained by (a) the original model, and (b) the in-phase model; (c) the phase plane plots and (d) spectra showing the oscillation frequencies of the two plates oscillating in the out-of-phase and in-phase modes; (e) the oscillation modes of plate 1 when the two plates oscillate in the out-of-phase mode, and (f) in the in-phase mode. In subfigures (c) and (d), the lines with various symbols: circle, original model, plate 1; diamond, original model, plate 2; up triangle, in-phase model, plate 1; down triangle, in-phase model, plate 2.

As one can observe in Figs. 7(a) and (b), the amplitude of the out-of-phase oscillations is larger than that of the in-phase oscillations. This is because the value of the out-of-phase critical point is smaller than the in-phase one, as shown in Figs. 4(a) and (b). When oscillating in phase, the dynamics of either of the two plates is exactly the same, except that the transverse displacements of plate 2 have a constant part d_P; and either plate undergoes symmetrical oscillations with respect to its own neutral plane (i.e., the $Y = 0$ plane for plate 1 or the $Y = D_P$ plane for plate 2). On the other hand, when the two plates oscillate out of phase, the dynamics of either plate is the mirror image of the other one. However, as one can see in Figs. 7(a), (c) and (e), as well as more clearly in Fig. 5(a), the oscillations of either plate are not symmetrical with respect to its own neutral plane; a small buckling in the direction away from the other plate is superposed on the limit cycle oscillations. Regardless of the difference discussed above, one can see in Fig. 7 that the dynamics of the two-plate system, obtained with either the original or in-phase model, is qualitatively the same in terms of the time history, flutter frequency and oscillation modes. Additionally, as compared to the one-plate system with the same parameters (excepting d_P) studied in Ref. [2], the dynamics of either of the two plates in Fig. 7 is qualitatively the same.

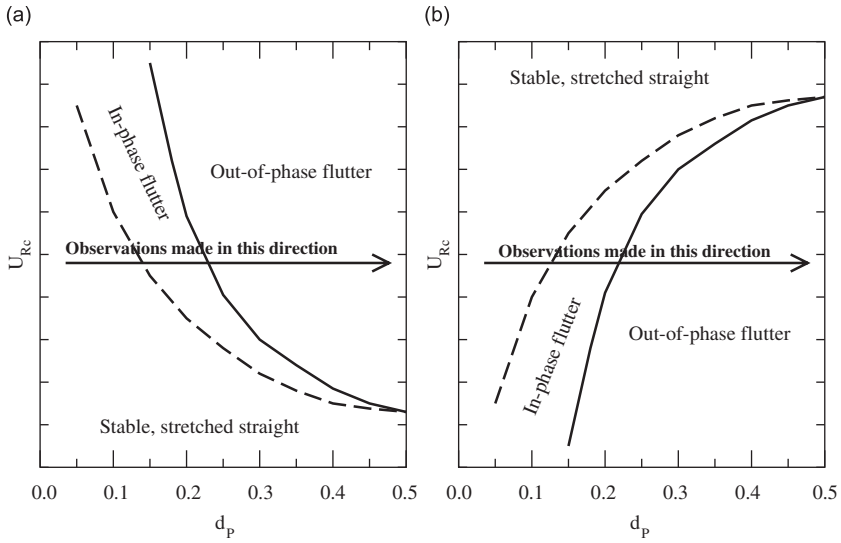

Fig. 8. Stability diagrams sketched according to the information published by Zhang et al. [6] and Farnell et al. [7]. Dashed line, the instability boundary of the in-phase mode; solid line, the instability boundary of the out-of-phase mode.

It is of interest to compare the results obtained by the present theory with previous experimental observations of Zhang et al. [6] and theoretical predictions of Farnell et al. [7] for the "two-plate" system in axial *channel* flow, where both in-phase (without the aid of virtual springs) and out-of-phase oscillations are reported: as illustrated in Fig. 8, when the channel size and the flow velocity are fixed, in-phase oscillations are observed when the separation between the two plates is small, while the two plates oscillate in the out-of-phase mode as the separation exceeds a certain value; moreover, as the separation is increased further, the two plates oscillate independently. A close examination of the two stability diagrams in Fig. 8 sketched according to the information published by Zhang et al. [6] and Farnell et al. [7], one may exclude the case shown in Fig. 8(b) because the two-plate system with fixed values of channel size and separation distance, is unlikely to remain in the stretched-straight state at a higher flow velocity but flutter at a lower one. Therefore, one can infer from Fig. 8(a) that the out-of-phase mode has a higher flutter threshold than the in-phase mode, which is completely opposite to the results obtained in the present paper. The underlying mechanism of this qualitative difference may be very complicated. However, a possible explanation is that, in the present paper, the fluid flow is supposed to be inviscid and the two plates are in unconfined axial flow. In the experiments conducted by Zhang et al. [6] and the theory of Farnell et al. [7] based on a Navier–Stokes solver, however, both viscosity and confinement are naturally in place in the experiments or taken into account in the analytical model. Moreover, the channel size is indeed small in the work of Zhang et al. [6] and Farnell et al. [7]; say, not as large as 1 when normalized using the plate length, and the channel size is fixed when the separation distance between the two plates is altered. Therefore, the viscosity of the fluid and the separation distance between the two plates, as well as between each plate and either of the upper/lower channel walls, may well have a profound and complex influence on the dynamics of the system.

4. Conclusions

The coupled dynamics of two cantilevered flexible plates aligned parallel to each other in open axial flow has been studied in this paper. It has been found that the two-plate system can oscillate in both in-phase and out-of-phase modes; and the in-phase modes are always more stable than the out-of-phase modes. When the separation is sufficiently large, the coupling between the two plates diminishes, and each plate oscillates independently like a one-plate system. As compared to the one-plate system, with decreasing inter-plate separation, the two-plate system becomes increasingly less stable in the out-of-phase mode; while, on the contrary, it becomes increasingly more stable in the in-phase mode. No matter whether the two plates

oscillate out of phase or in phase, the oscillation modes of either plate are qualitatively the same as their counterparts in the one-plate system. However, the plates undergo symmetrical oscillations with respect to the flow axis when they oscillate in phase; while, when the two plates oscillate out of phase, the dynamics of either plate is the mirror image of the other one; a buckling component in the direction away from the other plate can be observed in association with the limit cycle oscillations.

The oscillations of the two plates in the out-of-phase mode can naturally be predicted through numerical simulations; while those in the in-phase mode have to be obtained using artificial constraints (i.e., the virtual spring connections) applied to the system. Using the original model and the in-phase model with the virtual spring connections, it has been demonstrated that the dynamics of the two-plate system has two branches: one is stable in the out-of-phase mode with a lower flutter threshold, and the other one is unstable in the in-phase mode with a higher flutter threshold. Accordingly, the bifurcation diagram of a two-plate system can be divided into three regions as the flow velocity is increased: (i) the stable stretched-straight state, (ii) the region involving the coexistence of a stable limit cycle and an unstable stretched-straight state, and (iii) the region of coexistence of a stable and an unstable limit cycle oscillations. To the authors' best knowledge, this is the first time that one can capture an unstable branch of dynamics through direct numerical simulations.

Acknowledgements

The authors gratefully acknowledge the support by the Natural Sciences and Engineering Research Council of Canada (NSERC) and Le Fonds Québécois de Recherche sur la Nature et les Technologies (FQRNT) of Québec; the leading author also gratefully acknowledges the NSERC post-doctoral fellowship.

References

[1] L. Tang, The Dynamics of Two-Dimensional Cantilevered Flexible Plates in Axial Flow and a New Energy-Harvesting Concept, PhD Thesis, McGill University, Montréal, Québec, November 2007.
[2] L. Tang, M.P. Païdoussis, On the instability and the post-critical behavior of two-dimensional cantilevered flexible plates in axial flow, *Journal of Sound and Vibration* 305 (2007) 97–115.
[3] L. Tang, M.P. Païdoussis, The dynamics of two-dimensional cantilevered plates with an additional spring support in axial flow, *Nonlinear Dynamics* 51 (2008) 429–438.
[4] L. Tang, M.P. Païdoussis, J. Jiang, Dynamics of variants of two-dimensional cantilevered thin flexible plates in axial flow, *Journal of Sound and Vibration*, in press, doi:10.1016/j.jsv.2008.12.020.
[5] C.Q. Guo, M.P. Païdoussis, Analysis of hydroelastic instabilities of rectangular parallel-plate assemblies, *ASME Journal of Pressure Vessel Technology* 122 (2000) 502–508.
[6] J. Zhang, S. Childress, A. Libchaber, M. Shelley, Flexible filaments in a flowing soap film as a model for one-dimensional flags in a two-dimensional wind, *Nature* 408 (2000) 835–839.
[7] D.J.J. Farnell, T. David, D.C. Barton, Coupled states of flapping flags, *Journal of Fluids and Structures* 19 (2004) 29–36.
[8] J. Katz, A. Plotkin, *Low-Speed Aerodynamics*, second ed., Cambridge University Press, New York, 2001.
[9] Z.X. Yao, D.D. Liu, Vortex dynamics of blade–blade interaction, *AIAA Journal* 36 (4) (1998) 497–504.
[10] K.D. Jones, M.F. Platzer, Time-domain aeroelastic analysis of a two airfoil system with application to unsteady rotary wing flowfields, AIAA Paper No. 95-0337.
[11] K.D. Jones, M.F. Platzer, Numerical computation of flapping-wing propulsion and power extraction, AIAA Paper No. 96-0826.